Arch. Mech., 37, 6, pp. 573–585, Warszawa 1985

Simulation of material behaviour of alloys with shape memory

M. ACHENBACH and I. MÜLLER (BERLIN)

THE PAPER presents a model that is capable of simulating the complex load-deformation-temperature behaviour of memory alloys. The structure of the model is such that it reflects the known microscopic properties of the metallic lattice of such alloys. In particular, the basic element of the model is capable of assuming different configurations that duplicate the austenitic lattice structure and its martensitic twins. The phase transformations occurring in memory alloys are mathematically described here by evolution equations for the phase fractions, and the temperature of the model is governed by the energy equation. The interfacial energy between martensitic and austenitic lattice layers is taken into account in the calculation of the transition probabilities that determine the evolution of the phase fractions. This effect tends to stabilize the austenitic phase in the high temperature range and at small loads.

Przedstawiony w pracy model jest w stanie symulować złożone zależności „obciążenie-odkształcenie-temperatura" zachodzące w stopach z pamięcią. Struktura modelu odzwierciedla znane własności mikroskopowe takich stopów. W szczególności, podstawowy element modelu jest zdolny przyjmować różne konfiguracje naśladując strukturę sieci austenitycznej i jej martenzytycznych bliźniaków. Przemiany fazowe występujące w stopach z pamięcią opisane są tu matematycznie przez równania ewolucji faz, a temperatura modelu opisana jest przez równanie energii. Energię powierzchni rozdziału między warstwami martenzytycznymi i austenitycznymi uwzględniono przy obliczaniu prawdopodobieństwa przemian fazowych określających ewolucję faz. Zjawisko to wywiera działanie stabilizujące na fazę austenityczną w zakresie wysokich temperatur i małych obciążeń.

Представленная в работе модель в состоянии имитировать сложные зависимости „нагрузка-деформация-температура", имеющие место в сплавах с памятью. Структура модели отображает известные микроскопические свойства таких сплавов. В частности, основной элемент модели способен принимать разные конфигурации, подражая структуру аустенитной решетки и ее мартенситных двойников. Фазовые превращения, выступающие в сплавах с памятью, описаны здесь математически уравнениями эволюции фаз, а температура модели описана уравнением энергии. Энергия поверхности раздела, между мартенситными и аустенитными слоями, учтена при расчете вероятности фазовых превращений, определяющих эволюцию фаз. Это явление совершает стабилизирующее действие на аустенитную фазу в интервале высоких температур и малых нагрузок.

1. Typical load-deformation-temperature behaviour

1.1. Load-deformation curves

MEMORY alloys are characterized by a strong dependence of the load-deformation curves on temperature. Figure 1 shows schematic plots of such curves for increasing temperatures from T_1 through T_4.

At low temperatures there is an initial elastic curve through the origin, and there is a yield limit. The behaviour is much like that of a plastic body except that there exists a second elastic line along which the body can be loaded elastically far beyond the yield limit. Upon unloading there is a residual deformation. In Figs. 1a and 1b we see typical

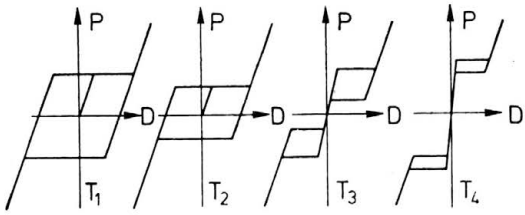

FIG. 1. Schematic load deformation curves for memory alloys.

hysteresis loops around the origin that reflect this behaviour. An increase of temperature decreases the width of the hysteresis.

At high temperatures there are two hysteresis loops in the first and third quadrant of the load-deformation diagram. There is still an initial elastic line, a yield limit and a second elastic line but, unlike at low temperatures, there is also a recovery limit at which large deformations are recovered upon a small decrease of the load. This phenomenon is called pseudoelasticity because, although there is a hysteresis, there is no residual deformation. Figs. 1c and 1d show this behaviour, and we can see that both the yield limit and the recovery limit tend to grow with increasing temperature while the hysteresis becomes smaller.

Typically the temperature between T_1 and T_4 is 30 K around room temperature and the maximum recoverable deformation is about 6%.

The memory of the material is implied by the diagram of Fig. 1: Suppose the body has been left at low temperature with a residual deformation where the right elastic branch intersects the D-axis. Upon heating to the temperature T_3, the body will creep back to the origin because $D = 0$ is its only possible deformation as long as no load is applied. The corresponding change of deformation is called the "recoverable memory deformation".

Information about theory and experiment in memory alloys can be obtained from the proceedings [1] and [2] of meetings on shape memory and martensitic transformations.

1.2. Combined dynamical and thermal loading

The curves of Fig. 1 show the result of quasi-static experiments with one parameter fixed, namely the temperature. A more complex picture appears when load and temperature change simultaneously. An instructive example of this type is provided by the standard test program of H. EHRENSTEIN [3] for the determination of the elastic deformation "recoverable memory" part of the deformation. In this program a triangular tensile load of constant amplitude and 0.05 Hz is applied to the specimen which is subject to a temperature cycle by external heating and subsequent cooling. Figure 2 shows in its upper part the applied load as a function of time and the single line curve in the lower part represents the temperature during the test. The resulting deformation is given by the zig-zag curve in the lower part of the figure. We observe that at low temperature the deformation of the specimen oscillates along the load around a large mean value. As the temperature increases, the deformation decreases drastically and ends up oscillating around a low mean value. As the temperature returns to its former value, the deformation increases again.

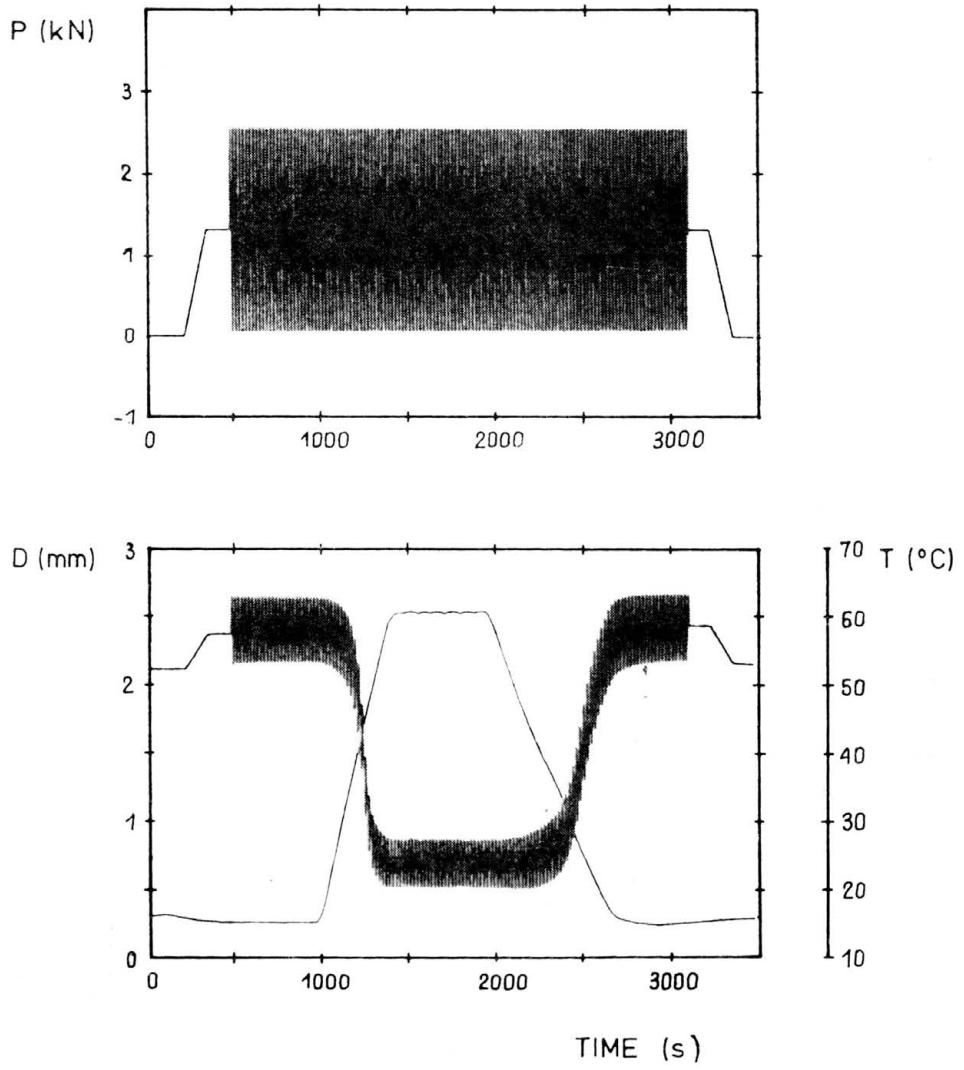

FIG. 2. Standard test program for the determination of elastic and recoverable plastic deformations.

1.3. Phase transformations

The physical reason for yield and recovery in a memory alloy is an austenitic-martensitic phase transformation and the twin formation in the martensitic phase. The martensite is stable at low temperatures and on the elastic curves of Figs. 1a and 1b we have equal proportions of martensitic twins while on the left and right elastic curve one or the other twin prevails. Austenite will form in bodies under small loads at high temperature. In Figs. 1c and 1d, for instance, the initial elastic curves refer to an austenitic body. Even at high temperature, however, the body can be forced to become martensitic by a large enough load and therefore the lateral elastic curves in Figs. 1c and 1d refer to a martensitic body.

Accordingly we may interpret the large deformations of Fig. 2 pertaining to low temperatures as deformations of a martensitic body with one twin only. The sharp decrease of deformation upon heating is due to the formation of austenite.

2. The model

2.1. Basic element

As the basic element of the model we envisage a small part of the metallic lattice which we call a lattice particle. Such a particle is shown in Fig. 3 in three equilibrium configurations denoted by $M_\pm$ and A. The particle A shows the highly symmetric austenitic phase

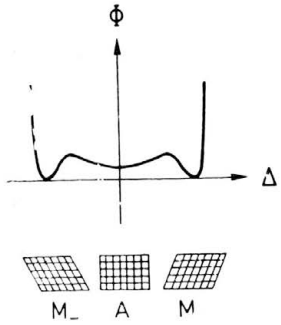

FIG. 3. Lattice particles and their potential energy.

while particles $M_\pm$ represent the martensitic phase. Obviously we may think of $M_\pm$ as sheared versions of A.

Intermediate shear lengths Δ are also possible and Fig. 3 shows the postulated form of the corresponding potential energy. The central minimum corresponds to the metastable equilibrium of the particle A and the lateral minima correspond to the stable martensitic equilibria. In between the minima we have energetic barriers.

If a lattice particle is subject to a shear load P, the potential energy of the load must be taken into account. That energy is a linear function of the shear length and therefore the potential energy of the particle is deformed by the addition of the line $-P\Delta$ as shown

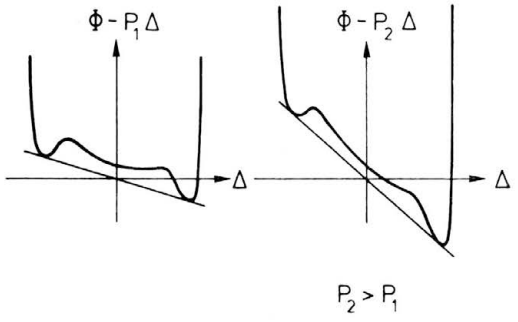

FIG. 4. Potential energy of a lattice particle under a shear load P.

in Fig. 4 for two different loads. Obviously the depths of the potential wells and the height of the barriers are affected by the load.

2.2. The body as a whole

To form a model for the body as a whole we arrange the lattice particles in layers and stack the layers as shown in Fig. 5a where a body is formed by alternating layers of M_+ and M_-.

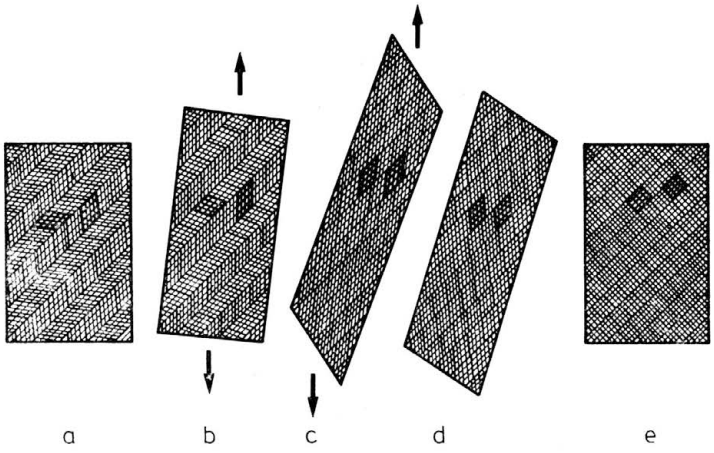

FIG. 5. Model for the body built from martensitic and austenitic layers.

The other bodies in Fig. 5 are supposed to give a qualitative idea of the modes of deformation that the model can simulate. Thus Fig. 5b shows the body under a small tensile load what makes the M_+ layers flatter and the M_- layers steeper. Both shear deformations contribute their vertical components Δ_i^v to the total deformation which thus becomes

$$D = \sum_i \Delta_i^v, \tag{2.1}$$

where the sum extends over all layers. Removal of the loads makes all particles return to their old positions and therefore deformations under small loads are elastic.

When the applied load grows beyond a certain limit, the M_- particles will be so steep as to become unstable and they will flip into the M_+ position. The accompanying large shear length will be carried into the total deformation D which increases drastically as shown in Fig. 5c. Removal of the load now will bring all particles into their equilibrium M_+ positions so that the residual deformation of Fig. 5d remains.

When the so-deformed martensitic body is heated, the layers will assume the regular austenitic structure and therefore the body will appear as in Fig. 5e. A subsequent cooling will convert the particles back into M_+ and M_- and, in general, it will produce equal numbers of both twins so that we are back to the configuration of Fig. 5a.

Thus we see how the various modes of deformation are simulated by the model: elastic deformation is due to a shearing of lattice particles, yield occurs during flippling and residual deformation results upon unloading after flipping. The recovery is achieved by the rearrangement of particles in the high temperature phase.

2.3. Polycrystalline body

The above-described model has been considerably refined so as to apply to polycrystalline bodies in plane strain situations. That refinement is the subject of a recent paper [4] to which the interested reader is referred for details. In this paper the measure D for deformation, see Sect. 2.1, is replaced by a proper deformation gradient and the rotation of lattice particles during the deformation is taken into account.

The numerical results presented below have all been gained for this more complex model even though a single crystal structure and a uniaxial load was assumed. However, for greater clarity in the explanation we proceed to describe the simple model of Sect. 2.2.

3. Rate laws for phase fractions and temperature

3.1. Qualitative description of the effects of temperature

Temperature makes the lattice particles fluctuate in their potential wells so that the faster ones may occasionally overcome the energetic barriers. Figure 6 shows the situation suggestively by representing the various lattice particles as dots in the neighbourhood of

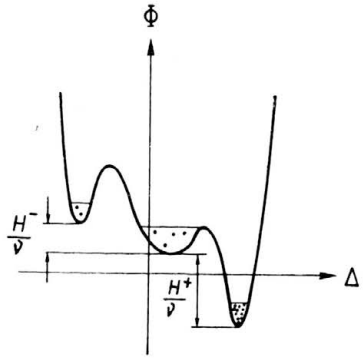

FIG. 6. Distribution of lattice particles among the potential wells.

the minima of the potential energy curve. The height of the pools of particles indicates the mean energy of fluctuation.

The fraction of particles in the different minima are denoted by $x^{\pm}$ and x^0 and they will be referred to as phase fractions of the martensitic twins and of austenite, respectively.

In the situation of Fig. 6 one does not specify the shear lengths of individual particles. Rather one determines the fraction $x_\Delta d\Delta$ of particles with shear lengths between Δ and $\Delta + d\Delta$. According to the rules of statistical mechanics, that fraction is proportional to the Boltzmann factor formed with the appropriate potential energy

$$x_\Delta d\Delta = C^{+0-} e^{-\frac{\phi(\Delta, P)}{kT}} d\Delta.$$

The factor of proportionality C may be different in the three potential wells, hence the indices $+0-$. They will generally be different at low temperature when no thermal equilibrium prevails between the phases. In that case C^{+0-} will essentially be determined by the phase fractions x^{+0-}.

From Eq. (2.1) it is obvious that the distribution of particles among the wells will determine the deformation D. Thus if all particles are in the right potential well, the body will be long as shown in Figs. 5c and 5d, while it will be in the short configuration 5a if the lateral minima have equal numbers of particles.

3.2. Rate laws for phase fractions

3.2.1. Without consideration of interfacial energies. As indicated before, there will generally be a transition of some particles across the energetic barriers and this will lead to a change of the phase fractions. A simple mathematical model for this kind of transition is furnished by the rate laws.

$$
\begin{aligned}
\dot{x}^- &= -x^- \overset{-0}{p} + x^0 \overset{0-}{p}, \\
\dot{x}^0 &= +x^- \overset{-0}{p} - x^0 \overset{0-}{p} - x^0 \overset{0+}{p} + x^+ \overset{+0}{p}, \\
\dot{x}^+ &= + x^0 \overset{0+}{p} - x^+ \overset{+0}{p}.
\end{aligned} \tag{3.1}
$$

According to Eq. $(3.1)_1$ the rate of change of x^- has two parts, a loss and a gain. The loss is due to particles that jump out of the M_- phase into the neighbouring A phase and their number is considered proportional to x^-, the fraction of particles M_-. The gain consists of particles that jump from A to M_- and accordingly it is proportional to x^0. The respective factors of proportionality are the transition probabilities $\overset{-0}{p}$ and $\overset{0-}{p}$, whose form will be discussed presently. Equations $(3.1)_{2,3}$ are similarly constructed except that Eq. $(3.1)_2$ has more terms since the central minimum can exchange particles with both adjacent minima. The transition probabilities for the jumps between A and M_+ are $\overset{0+}{p}$ and $\overset{+0}{p}$.

The transition probability $\overset{-0}{p}$ (say) is assumed to be proportional to the probability

$$
\frac{e^{-\frac{\Phi(m_L;\, P)}{kT}}}{\int_{-\infty}^{m_L} e^{-\frac{\Phi(\Delta;\, P)}{kT}}\, d\Delta} \tag{3.2}
$$

of a M_- particle to be on top of the left barrier whose abscissa is $\Delta = m_L$. To obtain the transition probability $\overset{-0}{p}$ from Eq. (3.2) we multiply by $\sqrt{(kT)/(2\pi m)}$, which is the mean speed of the fluctuating particles. Similar arguments refer to the other transitions and we obtain

$$
\begin{aligned}
&\overset{-0}{p} = \sqrt{\frac{kT}{2\pi m}}\,\frac{e^{-\frac{\Phi(m_L;\,P)}{kT}}}{\int\limits_{-\infty}^{m_L} e^{-\frac{\Phi(\Delta;\,P)}{kT}}\,d\Delta}, \qquad \overset{0-}{p} = \sqrt{\frac{kT}{2\pi m}}\,\frac{e^{-\frac{\Phi(m_L;\,P)}{kT}}}{\int\limits_{m_L}^{m_R} e^{-\frac{\Phi(\Delta;\,P)}{kT}}\,d\Delta},\\
&\overset{0+}{p} = \sqrt{\frac{kT}{2\pi m}}\,\frac{e^{-\frac{\Phi(m_R;\,P)}{kT}}}{\int\limits_{m_L}^{m_R} e^{-\frac{\Phi(\Delta;\,P)}{kT}}\,d\Delta}, \qquad \overset{+0}{p} = \sqrt{\frac{kT}{2\pi m}}\,\frac{e^{-\frac{\Phi(m_R;\,P)}{kT}}}{\int\limits_{m_R}^{\infty} e^{-\frac{\Phi(\Delta;\,P)}{kT}}\,d\Delta}.
\end{aligned}
\tag{3.3}
$$

3.2.2. With consideration of interfacial energies. The above calculation of the transition probabilities has not taken into account the change of interfacial energy that will generally go along with a change of phase fractions. However, it is intuitively clear that the formation of an interface will require energy and, in particular, this will be so for an austenitic-martensitic interface because of the different lattice structure. We proceed to introduce a correction of the transition probabilities that takes this effect into account.

We shall assume that the transition probabilities are of the form

$$
\overset{ij}{P} = \overset{ij}{p}\, e^{-\frac{\overset{ij}{\Delta}\Psi}{kT}}, \tag{3.4}
$$

where $\overset{ij}{p}$ stands for any one of the probabilities (3.3) and $\overset{ij}{\Delta}\Psi$ is the change of the interfacial free energy in the transition of a lattice particle from phase i to phase j.

The free energy associated to K interfaces between austenite and martensite (1) is equal to

$$
\Psi = KE - kT \ln \binom{N^0}{K/2} \binom{N-N^0}{K/2}, \tag{3.5}
$$

where E is the energy of one interface. N^0 and $N-N^0$ are the numbers of austenitic and martensitic layers, respectively. The second term in Eq. (3.5) represents the configurational entropy of the interfaces.

Unfortunately there is no unique relation between the number K of interfaces and the phase fractions $x^{\pm 0}$. Indeed, for given values of $x^{\pm 0}$ we can obviously have many different interfaces. However, we may argue that the expectation value of K is the one which makes Ψ a minimum. By Eq. (3.5) this gives (2)

$$
K_{\min} = \frac{N}{1 - e^{-\frac{2E}{kT}}} \left[1 - \sqrt{1 - 4x^0(1-x^0)\left(1 - e^{-\frac{2E}{kT}}\right)} \right]. \tag{3.6}
$$

(1) Interfaces between martensitic twins are not considered in the calculation of the free energy.

(2) The Stirling formula has been used in the derivation of Eq. (3.6).

The corresponding minimal value of Ψ will be used in Eq. (3.4), viz.,

$$\Psi_{\min} = K_{\min}E - NkT\left[x^0\ln x^0 + (1-x^0)\ln(1-x^0) - \left(x^0 - \frac{K_{\min}}{2N}\right)\ln\left(x^0 - \frac{K_{\min}}{2N}\right) - 2\frac{K_{\min}}{2N}\ln\frac{K_{\min}}{2N} - \left(1-x^0-\frac{K_{\min}}{2N}\right)\ln\left(1-x^0-\frac{K_{\min}}{2N}\right)\right]. \tag{3.7}$$

The calculation of $\overset{-0}{\Delta}\Psi$ (say) proceeds as follows. We have

$$\begin{aligned}\overset{\pm 0}{\Delta}\Psi &= \Psi_{\min}\left(x^0 + \frac{1}{N}\right) - \Psi_{\min}(x_0),\\ \overset{\pm 0}{\Delta}\Psi &= \frac{\partial\Psi_{\min}}{\partial x^0}\frac{1}{N},\end{aligned} \tag{3.8}$$

and, accordingly, the transition probability $\overset{\pm 0}{P}$ reads

$$\overset{\pm 0}{P} = \overset{\pm 0}{p}\exp\left\{-\frac{1}{kT}\left(\frac{E}{N}\frac{\partial K_{\min}}{\partial x_0} - kT\left[\ln\frac{x^0\left(1-x^0-\frac{K_{\min}}{2N}\right)}{(1-x^0)\left(x^0-\frac{K_{\min}}{2N}\right)} + \frac{1}{N}\frac{\partial K_{\min}}{\partial x_0}\cdot\ln\frac{\left(x^0-\frac{K_{\min}}{2N}\right)\left(1-x^0-\frac{K_{\min}}{2N}\right)}{\left(\frac{K_{\min}}{2N}\right)^2}\right]\right)\right\}. \tag{3.9}$$

$\overset{0\pm}{P}$ results from Eq. (3.9) by replacing $\overset{\pm 0}{p}$ by $\overset{0\pm}{p}$ and by changing the $-$sign in the exponent into a $+$sign.

3.3. Rate law for temperature

The proposed rate law for temperature is nothing else but the balance of energy applied to the body in thermal contact with its environment and in the process of a phase change. We write

$$C\dot{T} = -\alpha(T-T_E) - \left(\dot{x}^- H^-(P) + \dot{x}^+ H^+(P)\right), \tag{3.10}$$

where C is heat capacity, α is the coefficient of heat transfer from the body to the environment whose temperature is T_E. The quantities $H^{\pm}$ in Eq. (3.10) are the latent heats for the phase transitions from $M_{\pm}$ to A. If ν is the number of lattice particles, we have

$$H^{\pm}(P) = \nu\left(\Phi(\Delta^{\pm}; P) - \Phi(\Delta^0; P)\right), \tag{3.11}$$

where $\Delta^{\pm 0}$ denote the positions of the minimum of $\Phi(\Delta; P)$.

3.4. Deformation

In the case of thermally fluctuating particles the deformation cannot be calculated from Eq. (2.1) since the shear lengths of individual particles are unknown. The equivalent to Eq. (2.1) in the present case is the formula

$$(3.12)\quad \frac{\sqrt{2}D}{N} = x^{-}\frac{\int_{-\infty}^{m_L} \Delta e^{-\frac{\Phi(\Delta;P)}{kT}}\,d\Delta}{\int_{-\infty}^{m_L} e^{-\frac{\Phi(\Delta;P)}{kT}}\,d\Delta} + x^{0}\frac{\int_{m_L}^{m_R} \Delta e^{-\frac{\Phi(\Delta;P)}{kT}}\,d\Delta}{\int_{m_L}^{m_R} e^{-\frac{\Phi(\Delta;P)}{kT}}\,d\Delta} + x^{+}\frac{\int_{m_R}^{\infty} \Delta e^{-\frac{\Phi(\Delta;P)}{kT}}\,d\Delta}{\int_{m_R}^{\infty} e^{-\frac{\Phi(\Delta;P)}{kT}}\,d\Delta}.$$

Thus D appears as the sum of three terms of which each one represents the product of the number of particles in a phase and the expectation value of Δ in that phase. The $\sqrt{2}$ in Eq. (3.12) results from the arrangement of layers at an angle of 45° to the direction of the load.

4. Numerical exploitation of the model

4.1. Scope

The energy balance (3.10) and the rate laws for the phase factors (3.1), with $\overset{ij}{p}$ is replaced by $\overset{ij}{P}$ according to Eq. (3.9) and permit the solution of the following problem: *Determine $D(t)$ for given functions $T_E(t)$ and $P(t)$.*

The solution proceeds by stepwise integration of Eqs. (3.10) and (3.1) which gives us the temperature of the body $T(t)$ and the phase fractions $x^{\pm 0}(t)$. These functions and $P(t)$ are introduced into Eq. (3.12) to give $D(t)$.

4.2. Load deformation curves in tension and compression under isothermal conditions

The program described above is first carried out for constant values of T_E and a tension and compression cycle $P(t)$. The results of four such calculations are presented in the four sets of diagrams of Fig. 7. The applied load is the same one in all sets; it is represented by the $P(t)$ curves. Each set, however, refers to a different constant temperature T_E whose value is represented by the straight line in the (T, t)-diagram.

There result different functions for the phase factors $x^{\pm 0}(t)$ corresponding to the different temperatures T_E, and the temperature $T(t)$ of the model is represented by the kinky curves in the (T, t) -diagrams. The resulting deformation is shown in the (D, t) -diagrams.

It is particularly instructive to eliminate time between the two functions $P(t)$ and $D(t)$ to come up with a plot P vs. D which is also shown in Fig. 7. These load deformation curves must be compared to the schematic pictures of Fig. 1 and we observe good qualitative agreement.

Several features of the curves of Fig. 7 merit a comment:

First of all we see that at low temperatures the hysteresis loops contain the origin and that all aspects of the schematic pictures of Fig. 1 are present: initial elastic deformation, yield, second elastic line and residual deformation; the yield limit decreases with increasing temperature. At high temperatures we see the initial and the second elastic curve as well as yield and recovery just as experimentally observed. As temperature increases, the hysteresis becomes smaller and gets farther away from the origin.

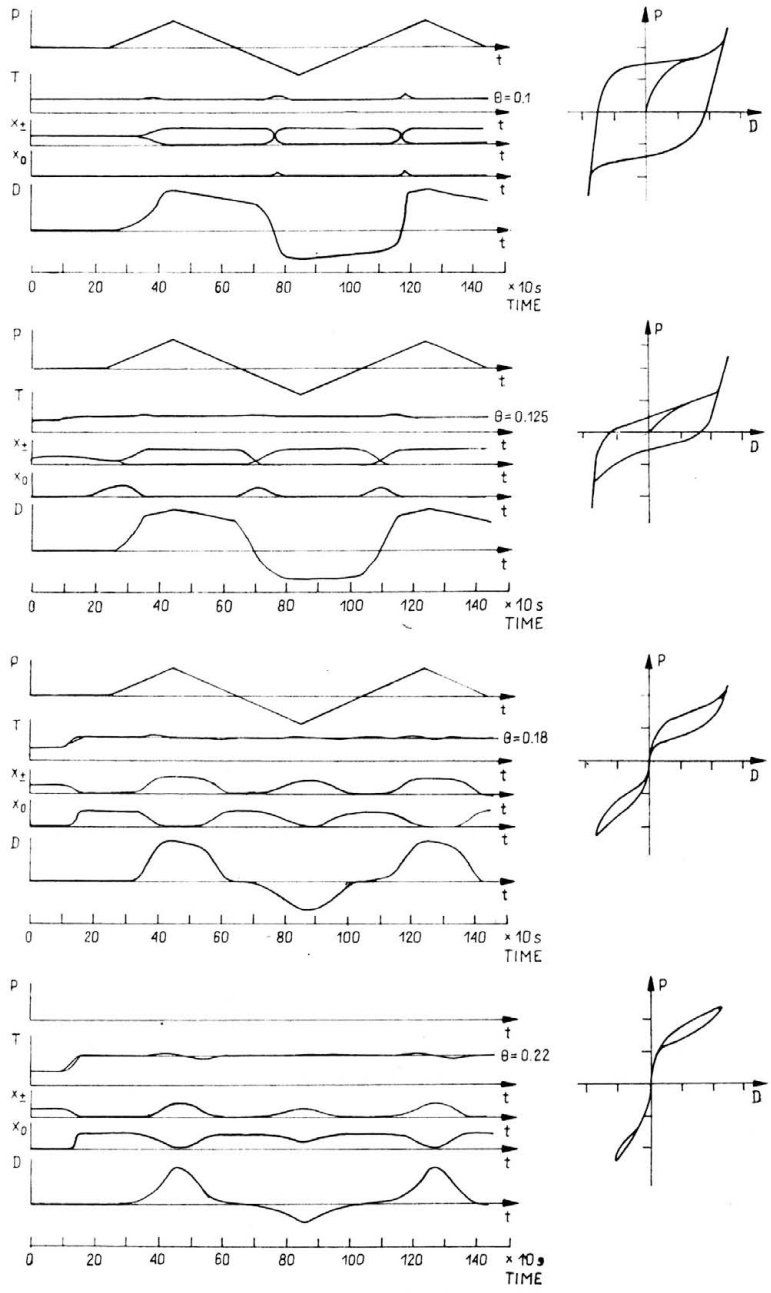

FIG. 7. Deformation $D(t)$ under a load $\boldsymbol{P}(t)$ at different temperatures (t).

Also, as expected, the deformation goes along with the changes in the phase factors; large positive and negative deformations are always linked to the prevalence of M_+ and M_- respectively. Small deformations can either be the result of a large fraction x^0 or else the result of like proportions x^+ and x^-. The former case will be realized at high temperatures and the latter at low temperatures.

Unlike the external temperature T_E, the actual temperature T of the body is not constant. In fact, T deviates from T_E whenever a rapid phase change occurs. This is due to the fact that the latent heat of the transformation is too big to be carried away immediately into the environment. It is interesting to observe that the body can not only be heated above T_E by a phase change but also cooled below T_E. This latter case will be most noticeable when austenite is formed from one of the martensitic twins while the body is still loaded.

The asymmetric character of the (P, D)-diagram in the tensile and compressive regions would not arise in the simple model that has been described in Chapter 2. However, as was mentioned before (see Sect. 2.3), all calculations have been performed by the use of the more refined model presented in [4] where such an asymmetry arises naturally because of the rotation of lattice layers in the deformation.

4.3. Combined dynamical and thermal loading

In order to show the quality of the model we choose a dynamical and thermal loading that is akin to those of the standard test program that was discussed in Sect. 1.2: An alternating tensile load of constant amplitude is applied and the temperature is first raised and then lowered. This "input" is shown in the first two diagrams of Fig. 8. The following

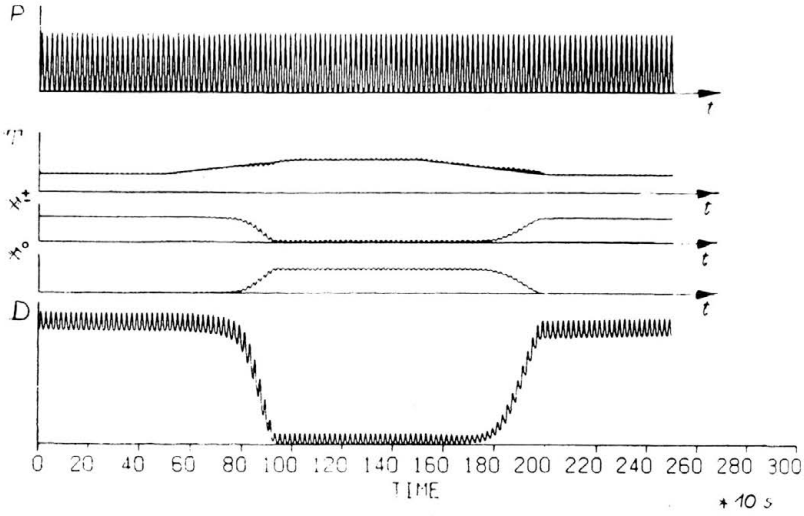

FIG. 8. Simulation of the standard test program and its outcome.

two diagrams represent the resulting phase factors. We can clearly observe how, with growing temperature, the initial martensitic state is changed into an austenitic one and — as temperature returns to small values — how martensite is formed.

The last diagram of Fig. 8 shows the deformation as it oscillates along with the load. At first, when the temperature is small, we have a large deformation. Upon heating the body contracts, always oscillating and it returns to the original value of deformation when the temperature falls again.

The parameters of the model have been chosen so as to match the $D(t)$ plot as similar as possible to the corresponding curve in Fig. 2. That this is possible speaks for the versatility of the model.

References

1. J. PERKINS (ed.), *Shape memory effects in alloys*, Plenum Press, New York, London 1975.
2. L. DELAEY, L. CHANDRASEKARAN (eds), Proc. Int. Conf. on Martensitic Transformation, Leuven 1982; J. Physique, **43**, 1982.
3. H. EHRENSTEIN, *Die Herstellung und das Formerinnerungsvermögen von NiTi*, Dissertation TU, Berlin 1985.
4. M. ACHENBACH, T. ATANACKOVIC, I. MÜLLER, *A model for memory alloys in plane strain*, Int. J. Solids and Structures (in press).

HERMANN FÖTTINGER INSTITUT, TECHNISCHE UNIVERSITÄT, BERLIN.

Received March 18, 1985.